Available online at www.sciencedirect.com
SCIENCE DIRECT®
Chaos, Solitons and Fractals 24 (2005) 1031–1045
CHAOS SOLITONS & FRACTALS
www.elsevier.com/locate/chaos

Fractal scaling and simulation of velocity components and turbulent shear stress in open channel flow

Ali Naghi Ziaei [a], Ali Reza Keshavarzi [a,*], Emdad Homayoun [b]

[a] *Water Department, Shiraz University, Shiraz, Iran*
[b] *Mechanical Engineering Department, Shiraz University, Shiraz, Iran*

Accepted 15 September 2004

Abstract

Fully developed turbulent flow indeed consists of a hierarchy of eddies or scales of various disorders. Due to the complexity of turbulence, the turbulent flow structure has not been completely understood. Thus, abundant empirical observations have been made about fractality in hydrodynamic turbulence. In this study, the fractal scaling of velocity components (u', v') and Reynolds shear stress ($u'v'$) for fully developed flow in an open channel were studied for Reynolds number in the range of 29,000–85,000.

An efficient algorithm was developed to construct Fractal Interpolation Functions (FIF). The algorithm was used to simulate more than 200,000 time series of u', v', and $u'v'$ that were measured in a laboratory flume. The algorithm was also used to compute fractal dimension. The fractal dimensions of the turbulent data were accurately obtained by applying only as few as 500 data points. It was found that the fractal dimension of u', v', and $u'v'$ were 1.615, 1.657, and 1.559, respectively. The relationships between the fractal dimension and Froude number (Fr) and Reynolds number (Re) were also investigated. It was found that the fractal dimension of turbulent data and Re and Fr were reasonably correlated.

Moreover, the fractal dimension of Reynolds shear stress in bursting events (outward interaction, ejection, inward interaction, and sweep) was calculated and compared with each other. There were some differences among the fractal dimension of Reynolds shear stress for four quadrants of bursting process. The fractal dimension of $u'v'$ in sweep and ejection events were more than the fractal dimension of the overall Reynolds shear stress.

1. Introduction

Turbulence is a natural phenomenon occurring in almost all fluid flowing in open channel. It is usually characterized by highly disordered and chaotic fluid motion over a wide range of length scales and frequencies. To introduce the structure of turbulent flow, the most appropriate definition was presented by Richardson [1], who was suggested that the structure of fully developed turbulent flow consists of a hierarchy of the eddies, or scales of various disorders.

* Corresponding author. Tel./fax: +98 711 228 6130.
E-mail address: keshavrz@shirazu.ac.ir (A.R. Keshavarzi).

0960-0779/$ - see front matter © 2004 Elsevier Ltd. All rights reserved.
doi:10.1016/j.chaos.2004.09.054

Additional studies by Einstein and Li [2] showed that the turbulent flow is a process with completely stochastic nature due to the intermittency of turbulent events.

Due to chaotic nature of turbulence, abundant empirical observations have been made about fractality in hydrodynamic turbulence. In particular, many works have investigated the fractal properties of various sets of physical interest in turbulence such as iso-concentration surfaces of advanced scalars e.g. Praskovsky et al. [3] and Sreenivasan and Meneveau [4] and vectors, or the structure of the spatial distribution of dissipation e.g. Meneveau and Sreenivasan, [5]. More directly related to the present subject matter, Scotti and Meneveau [6] showed that the turbulent velocity signals display fractal scaling with a fractal dimension of 1.7 ± 0.05. Scotti and Meneveau [7] used fractal interpolation function to construct a synthetic sub-grid for large eddy simulation (LES) of turbulence. Frisch et al. [8] applied fractal dimension to turbulent closure problems by providing a relation between fractal dimension and turbulence scales. Their model was used for near wall turbulence modeling by Jaw and Chen [9].

Furthermore, to define the coherent structure of turbulent flow, Kline et al. [10] was defined turbulence as a process, based on horizontal and vertical velocity fluctuation components (u' and v') in turbulent flows. The process consists of four different types of event, according to quadrant analysis of velocity fluctuations. These events are categorized as: the sweep ($u' > 0$, $v' < 0$), ejection ($u' < 0$, $v' > 0$), outward interaction ($u' > 0$, $v' > 0$) and inward interaction ($u' < 0$, $v' < 0$) in quadrant zones 4, 2, 1 and 3, respectively (Fig. 1).

To investigate the role of the bursting events in sediment entrainment and deposition, Bridge and Bennett [11] concluded that these four alternative types of bursting events have different effects on the mode and rate of sediment transport in open channel flow. Studies by, for example, Thorne et al. [12], Nelson et al. [13], and Drake et al. [14], Keshavarzi and Ball [15] indicated that close to the bed, sediment entrainment is mostly correlated with particular bursting events. Also, Nezu and Nakagawa [16] pointed out that the mechanism of turbulent flow and in particular bursting events over rough beds in open channel is associated with turbulence and momentum transfer and it is a process by which sediment particles are entrained from the bed and is transported with the flow.

The contributions of bursting events, such as the sweep and ejection events, to momentum transfer have been extensively studied by quadrant analysis or probability analyses based on two-dimensional velocity information. Studies by Nakagawa and Nezu [17] and Grass [18] have indicated that just above the channel bed, the sweep event is more responsible than the ejection event for transfer of momentum into the bed layer. Nakagawa and Nezu [17], Thorne et al. [12] and Keshavarzi and Ball [19,15] concluded that sweep and ejection event occurred more frequently than outward and inward interactions. Keshavarzi [20] showed that the average magnitude of the shear stress in a sweep event was 140% of the time average shear stress with the 30% frequency of occurrence. Therefore turbulence modeling based on time averaged properties cannot be used to detect the coherent structures [16].

The four types of bursting events identified earlier have different influences on the rate, and mechanisms of sediment entrainment in a turbulent flow. Despite the importance of the bursting events in sediment transport, the statistical characteristics of bursting events have not been investigated in sufficient detail.

In this study, an algorithm is developed to construct FIF. The developed algorithm was applied to model time series of turbulent data (i.e., u', v', and $u'v'$, horizontal and vertical velocity fluctuation components and turbulent shear stress, respectively). The velocity components were measured in a laboratory flume. The reliability of the algorithm for calculating the fractal dimension of data set is also scrutinized. Then, it was applied to calculate the fractal dimension of the turbulent data. The relationships between fractal dimension of the flow properties and Reynolds number and

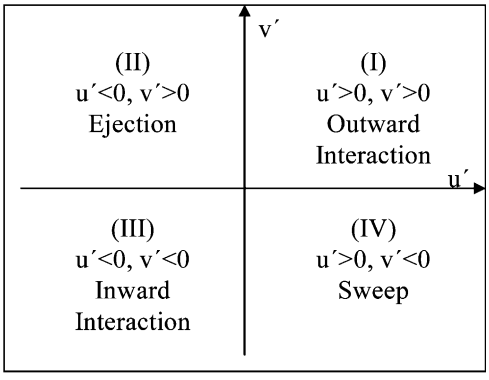

Fig. 1. Four class of bursting events and their associated quadrants.

Froude number are studied. Due to very important role of bursting process in turbulence specification, the fractal dimension of Reynolds shear stress of bursting events is also calculated.

2. Theoretical development of fractal model

Fractal geometry concerns with complicated subset of geometrically simple space such as R^2. In deterministic fractal geometry the focus is on the subsets of a space that are generated by simple contractive geometrical transformations of the space into itself. A general affine shear transformation can be defined as:

$$w_n\begin{pmatrix} x \\ y \end{pmatrix} = \begin{pmatrix} a_n & 0 \\ c_n & d_n \end{pmatrix}\begin{pmatrix} x \\ y \end{pmatrix} + \begin{pmatrix} e_n \\ f_n \end{pmatrix}, \tag{1}$$

where a_n, c_n, d_n, e_n, and f_n are transformation parameters. Here shear means that on the x-y plane, lines parallel to y-axis are mapped into lines parallel to y-axis. Every contractive mapping on a complete metric space has a fixed point on that metric space. The fixed point of the iterated function systems (IFS) is called the attractor. The attractor is the fractal object.

In order to show a very irregular and ragged curve of turbulence properties such as temporal variations of velocity fluctuation components and Reynolds shear stress are fractal objects, it should be accurately modeled by a set of self-affine maps. Fractal interpolation functions (FIF) are very powerful tools to model such curves. The graph of an FIF is the attractor of the IFS that passes through the given interpolation points (e.g., turbulent data points). In other words, FIF provides a new means for curve fitting to experimental data such as velocity components. Moreover, one can ensure that the fractal dimension of the graph of FIF agrees with that the data over an appropriate range of scales e.g. [21].

Let a set of data (interpolation points) be given. The attractor is the graph of a continuous function $f:[x_0, x_N] \to R$ which interpolates the data. If an IFS of the form $\{R^2; w_n, n = 1,2, \ldots, N\}$ is considered, where the maps are affine shear transformations, the transformations are constrained by the data according to:

$$w_n\begin{pmatrix} x_0 \\ F_0 \end{pmatrix} = \begin{pmatrix} x_{n-1} \\ F_{n-1} \end{pmatrix} \quad \text{and} \quad w_n\begin{pmatrix} x_N \\ F_N \end{pmatrix} = \begin{pmatrix} x_n \\ F_n \end{pmatrix} \quad \text{for } n = 1, 2, \ldots, N.$$

The situation is summarized in Fig. 2.

Let d_n be any real number, the above equations can always be solved for a_n, c_n, e_n, and f_n in terms of the data and d_n. i.e.,

$$a_n = \frac{x_n - x_{n-1}}{x_N - x_0}, \tag{2}$$

$$e_n = \frac{x_N x_{n-1} - x_0 x_n}{x_N - x_0}, \tag{3}$$

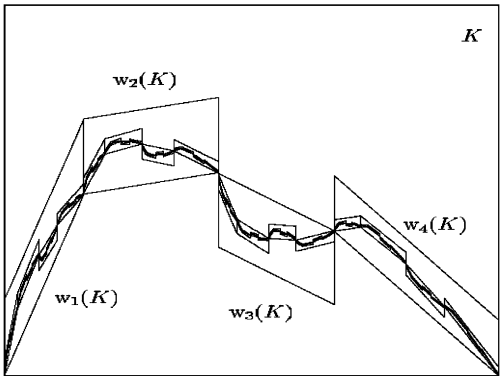

Fig. 2. Construction of FIF using IFS of shear transformation.

$$c_n = \frac{F_n - F_{n-1}}{x_N - x_0} - \frac{d_n(F_N - F_0)}{x_N - x_0}, \tag{4}$$

$$f_n = \frac{x_N F_{n-1} - x_0 F_n}{x_N - x_0} - \frac{d_n(x_N F_0 - x_0 F_N)}{x_N - x_0}. \tag{5}$$

Then the fractal dimension of the FIF can be calculated by:

$$\sum_{n=1}^{N} |d_n| a_n^{D-1} = 1 \quad \text{if} \quad \sum_{n=1}^{N} |d_n| > 1 \quad \text{and} \quad |d_n| \leqslant 1, \tag{6}$$

where D is the fractal dimension. Up to now it is explained how to calculate a_n, c_n, e_n, and f_n, but d_n, which is afterwards called vertical scaling factor (VSF) is unknown. Furthermore, for large number of data points, in order to model data in reasonable computation time, they should be categorized into fixed and target points. The fractal curve will pass through fixed points and approximate target points corresponding to accuracy of the calculated mapping parameters. Therefore, optimum number of fixed points (N) also should be specified.

Strahle [22] presented a simple method to calculate the VSF. To improve this method, Marvasti and Strahle [23] presented an algorithm which starts by categorizing the data into fixed and target points. But unlike the Strahle's method, the number of target points between each pair of fixed points is declared as a variable. This scheme is shown in Fig. 3. The dark solid points are the fixed points and the smaller ones are the target points. What remain to be determined are N and d_n. This scheme does not suggest any idea for selection of N, but the VSF is obtained by first drawing a line between the first and the last data point (i.e., (x_0, F_0), and (x_N, F_N)). Next the point which has the longest vertical distance to the line is calculated. The distance is designated as μ in Fig. 3 that can be positive (point above the line) or negative (point below the line). A line is then drawn between the fixed points on the nth interval ($1 \leqslant n \leqslant N$) and the distance of the farthest target point above or below this line is calculated. This is designated as v_n in Fig. 3. The vertical scaling factor is then defined as:

$$d_n = \frac{v_n}{\mu}. \tag{7}$$

Although this scheme does not have some of the previous method's difficulties, but the minimum number of essential target points to generate accurate model is unspecified.

Mazel and Hayes [24] presented both geometric and analytic methods to calculate the VSF. The geometric method is the same as Marvasti and Strahle method, but the analytic method is based on least square optimization. Furthermore, they presented an iterative algorithm to find both the optimum fixed points and the VSF for a given arbitrary data set. The algorithm is based on the property that the resulting fractal function is self-affine. By the collage theorem, if the interpolation points can be covered with affine transformation, and have the distance between the interpolation points and the collage of the function small, the attractor of the IFS will be a close approximation to the interpolation points. However, since the algorithm uses exhaustive search, it is too time consuming to be of practical use.

Vines [25] compared results of different methods for one-dimensional signal modeling. He suggested using local extremums of the data sequence as the fixed points of the transformations. These points are obtained by introducing some filters, and selecting those points which have the most deviation as extremums. He also showed that this method

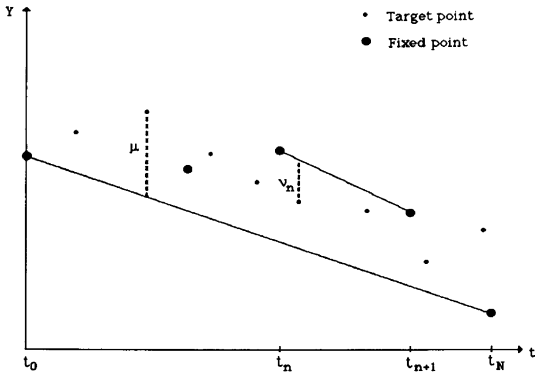

Fig. 3. Schematic of fixed points and target points.

was very efficient and the results were comparable with the exhaustive search. In this manner, even without the effect of the IFS, the model roughly follows the original data using a series of straight-line segments. Then the mapped data portion can be used to further increase the accuracy of the model. Due to advantages of the extremum approach, in this study it is used with a few improvements for selecting the fixed points. Marvasti and Strahle method was adopted for VSF calculation.

The Vines' extremum method and Mazel and Hayes algorithm were incorporated to develop an efficient algorithm for constructing a fractal model on the basis of iterated function systems. The developed algorithm provides suitable number of self-affine shear transformations that their attractor passes through the interpolation points during a very short time. The required computer program was developed using Matlab Language. Input file of the program includes horizontal and vertical velocity components (u and v) measured during a period of time in a laboratory flume in different distances from the bed.

In the program, after reading the input file, velocity fluctuation components (u', v') are calculated. Turbulent shear stress ($u'v'$) is calculated as multiplication of the velocity fluctuation components. Afterwards, according to sign of u' and v', $u'v'$ values are divided into four quadrants. $u'v'$ in different quadrants accompanied with their related time values are saved separately. Now time series of u', v', $u'v'$, quadrant 1, quadrant 2, quadrant 3 and quadrant 4 are ready to fractal modeling. The next step is determination of fixed points. In order to determine fixed points, the local extremums of the data sets are specified using a number of filters which are:

- The extremum is a point on which the sign of numerical derivative changes.
- Each maximum should be followed by a minimum and vise versa.
- Sequential extrema which have a specific trend should be removed i.e. (Fig. 4).

The number of transformations is equal to the number of sequential pairs of fixed points. To calculate the values of a_n, c_n, d_n, e_n, and f_n, after determination of fixed points, the data points between each pair of fixed points are specified. In other words, every data set is divided into N section (the number of maps or transformations). In each section the largest distance between the line that connect two endpoints of the section and the data points is computed. This value is called as v_n. Average value of all the calculated distances is also designated as g_n. Following calculation of μ, the value of d_n will be calculated by $d_n = v_n/\mu$ if $|d_n| \leqslant 1$ and $d_n = g_n/\mu$ if $|d_n| > 1$.

Having calculated values of mapping parameters a_n, c_n, e_n, and f_n, Eq. (6) is solved numerically to obtain fractal dimension. Afterwards, since mapping parameters and the number of maps is known, the fractal interpolation function can be constructed.

3. Data set description

In this study the turbulent data, which had been measured by Keshavarzi [19], were used. The data include time series of velocity components that are measured in experimental flume using 2D electromagnet velocity meter. Data sets comprised of different flow conditions in term of discharge, flow depth, velocity and in consequence, Reynolds and Froude numbers. Uniform and non-uniform conditions were stabilized by a tail gate installed at the end of the flume. Each test which was specified by a capital letter in Table 1, consisted of several time series of velocity components measured in different depths from the flume bed. Therefore, each data set has been named with a capital letter and a number which shows the distance in millimeter from the bed (e.g., K40).

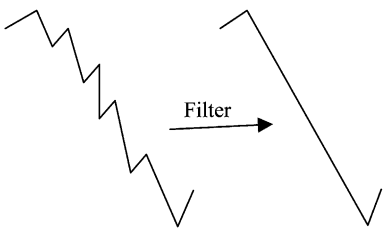

Fig. 4. Removing sequential extremums with a trend.

Table 1
Df_m for different flow conditions

Test	D	E	F	G	H	J	K	L	M	N	O	P	Q	V	W	Wb	X	Y	YY	Z
Discharge (l/s)	47	63.7	76.3	52	58	73.6	40.2	61	30.3	22	48.5	79.8	97.5	22.7	47.5	47.5	48.5	40.85	40.3	30.5
Depth (mm)	294	355	154	276	120	145	120	212	154	70	166	230	265	70	172	100	170	146	143	103
Temperature (°C)	15.5	15	15	15	15.5	14	13.5	13.5	13	12.2	13	13	12.6	24.4	24.4	24.4	18.6	19	19	19
Bed slope	0.005	0.005	0.005	0.005	0.005	0.005	0.005	0.005	0.005	0.005	0.005	0.005	0.005	0.005	0.005	0.005	0.005	0.005	0.005	0.005
Mean velocity (m/s)	0.26	0.29	0.81	0.31	0.79	0.83	0.55	0.47	0.32	0.52	0.48	0.57	0.60	0.53	0.45	0.78	0.47	0.46	0.46	0.49
Fr	0.15	0.16	0.66	0.19	0.73	0.70	0.51	0.33	0.26	0.62	0.38	0.38	0.37	0.64	0.35	0.79	0.36	0.38	0.39	0.48
Measurement rate (1/s)	10	10	10	10	10	10	10	10	10	10	10	10	10	10	10	10	10	10	10	10
Flow condition	S[a]&N[b]	S&N	S&U[c]	S&N	S&U	S&U	S&N	S& N	S&N	S&N	S&N	S&N	S&N	S&U	S&N	S&U	S&N	S&N	S&N	S&N
Re	39232	48258	83115	44750	68235	81778	47294	58994	33007	29333	51486	74579	85526	30267	49790	58642	51053	45288	44978	37377
$Df(u')$	1.556	1.382	1.402	1.501	1.675	1.584	1.778	1.713	1.745	1.723	1.733	1.730	1.737	1.532	1.492	1.474	1.641	1.680	1.672	1.672
$Df(v')$	1.638	1.589	1.448	1.536	1.651	1.620	1.747	1.708	1.767	1.765	1.773	1.778	1.764	1.558	1.567	1.544	1.704	1.690	1.668	1.692
$Df(u'v')$	1.573	1.520	1.418	1.505	1.604	1.582	1.681	1.667	1.648	1.632	1.695	1.682	1.674	1.491	1.503	1.488	1.634	1.654	1.634	1.627

[a] Steady.
[b] Non-uniform.
[c] Uniform.

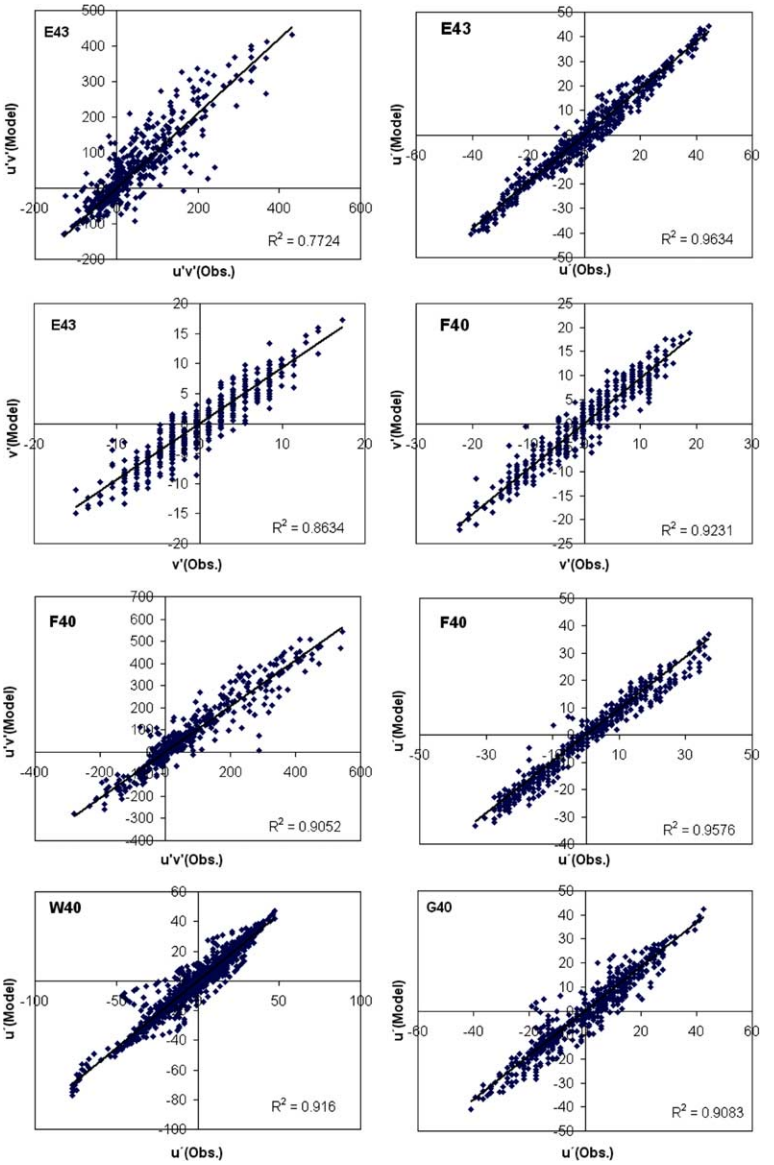

Fig. 5. Comparison between observed and computed (first iteration) turbulent data for some data sets.

4. Results and discussions

The result of this study can be categorized in three main parts as follow:

- turbulent data modeling,
- fractal dimension of turbulent data,
- fractal dimension of bursting events.

4.1. Turbulent data modeling

The model determined suitable local extremums for most data sets which roughly followed the original data. Therefore, it was expected that the attractor be close enough to the data set. The results of first iteration of the model are

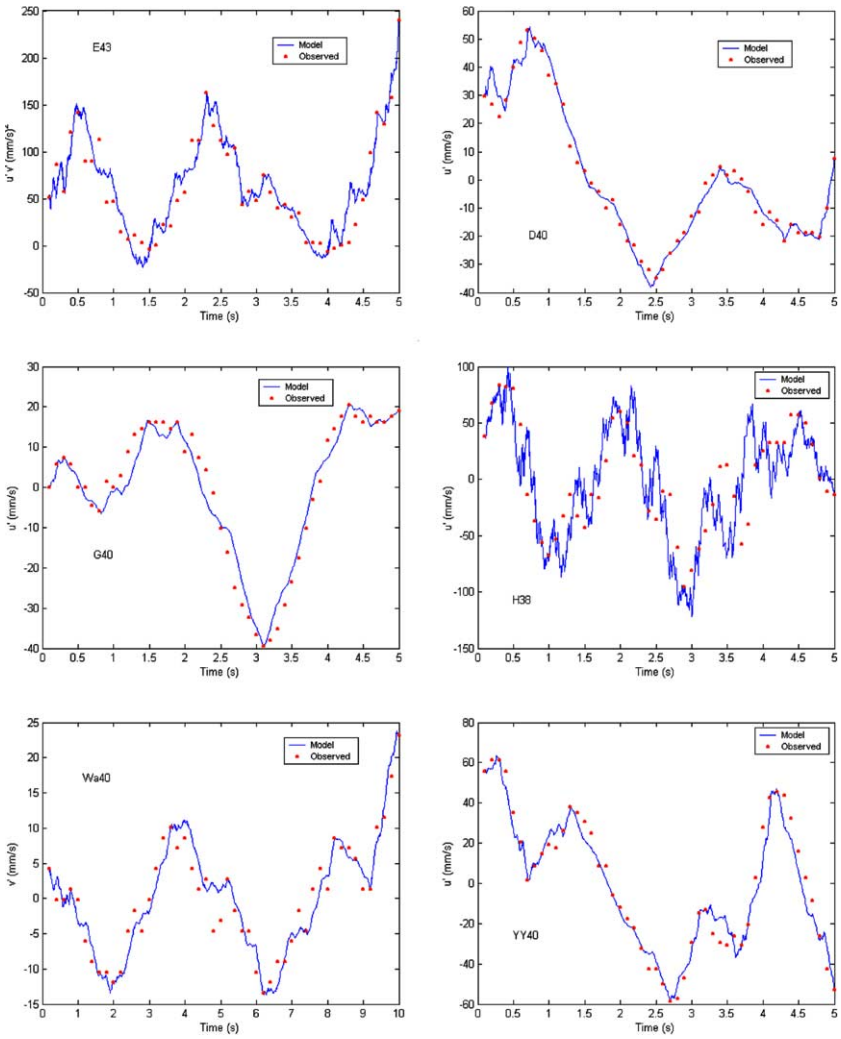

Fig. 6. Comparison between observed and modeled (five iteration) turbulent data for small parts of some data sets.

compared with measured turbulent data in Fig. 5. According to collage theorem, the closer this run of the model is to the data, the fractal interpolation function (attractor) closer to the given data set.

The results revealed good agreement between measured and simulated turbulent data. In some data set there exist some deviations which are to some extend because of unsuitable selected local extremums. Using more restricted filters may decrease these discrepancies. However, there exist some intrinsic differences between turbulence properties and fractal models.

Modeling the whole length of every data set was very time consuming. Thus only a small part of a couple of data sets was modeled. The computed fractal model using five iterations are compared with observed values for some data sets in Fig. 6.

The results showed that the fractal model was able to approximate turbulence properties with reasonable accuracy. Thus the temporal variation of velocity components and Reynolds shear stress displayed self-affinity over some scales. The results confirmed the previous studies e.g. Sreenivasan and Meneveau [4], Frederiksen et al. [26].

4.2. Fractal dimension of turbulent data

The Strahle [22] and Marvasti and Strahle [23] methods were used to calculate VSF, and in consequence the fractal dimension. However, they required great number of data points to calculate accurate fractal dimension. Furthermore,

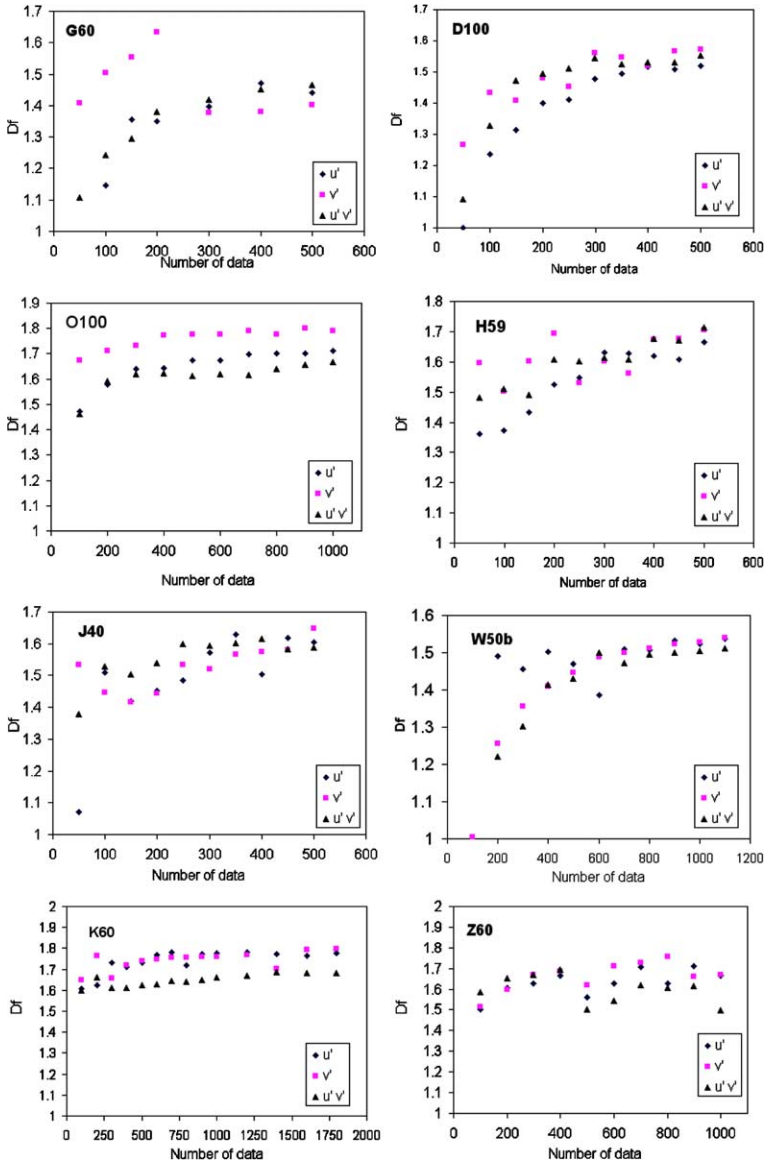

Fig. 7. Fractal dimension versus number of data points for some data sets.

for some data sets the absolute value of calculated d_n was greater than unity which was unacceptable. Therefore, the developed algorithm was utilized to compute the fractal dimension of turbulent data. In Fig. 7 the fractal dimension, calculated by the algorithm, versus the number of data points is plotted. The fractal dimension reached a constant value with about 500 data points. Therefore, the presented model is not only able to compute accurate fractal dimension with only 500 turbulent data points, but also it can be a good substitution for the Box-counting method because of unreliability of the latter method due to the elusiveness of the flat region on the logarithmic plot [23].

The fractal dimension of all turbulent data sets were calculated. Fig. 8 depicts fractal dimension versus normalized depth (d/H). It seems that there are not any specific relation between fractal dimension and distance from the bed. The calculated fractal dimensions of u', v', and $u'v'$ for all data sets were separately averaged to calculate the mean fractal dimension of turbulence properties. The mean fractal dimension of u', v', and $u'v'$ regardless of flow conditions were found to be 1.615, 1.657, and 1.559, respectively. The fractal dimension (Df) of each test, averaging from fractal dimension of turbulent data of different depths at which velocity measurements were made, and related flow conditions are tabulated in Table 1. These values are plotted versus Reynolds and Froude numbers in Figs. 9 and 10, respectively.

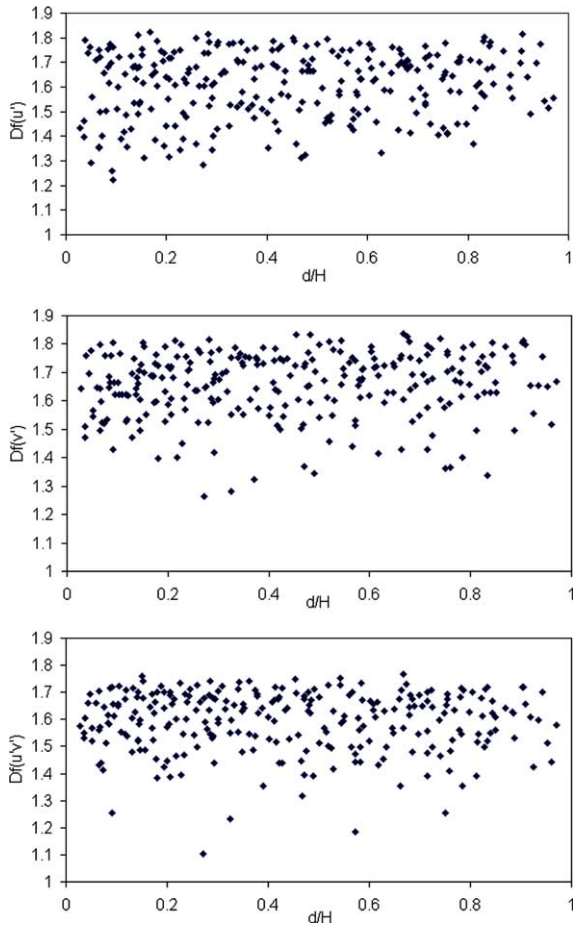

Fig. 8. Fractal dimension versus normalized depth.

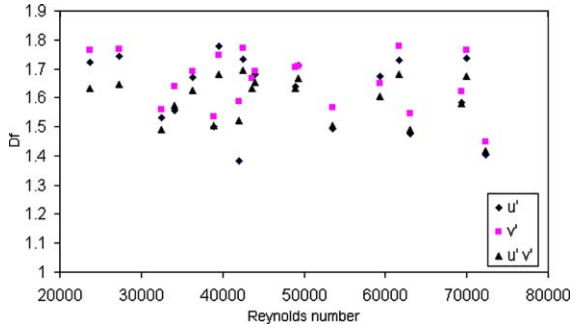

Fig. 9. Fractal dimension versus Reynolds number.

The result showed that there was not obvious relationship between *Df* and Reynolds number (*Re*), while *Df* and Froude number (*Fr*) were somehow correlated. It seems that fractal dimension is independent of Reynolds number. The results can be reasonable due to dominancy of gravity force in open channel flows. The curve of fractal dimension versus *Fr* consisted of two increasing and decreasing limbs. The decreasing limb belongs to uniform flow conditions. In uniform flow, declining of turbulence intensity and in consequence the fractal dimension of turbulent data seems reasonable due to more uniformity of velocity profile in comparison to non-uniform flow. To enhance the difference be-

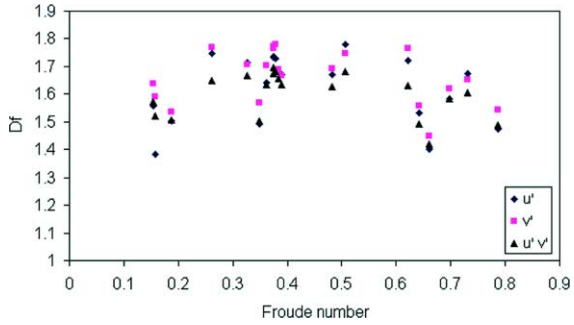

Fig. 10. Fractal dimension versus Froude number.

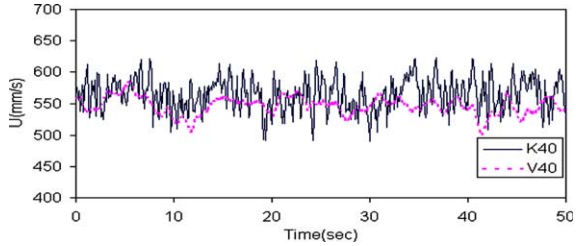

Fig. 11. Comparison between time series of observed horizontal velocity component in uniform and non-uniform flow conditions.

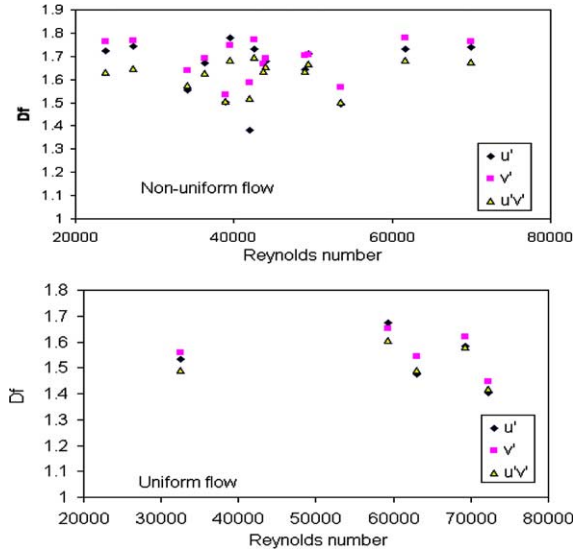

Fig. 12. Relationship between fractal dimension and Reynolds number in uniform and non-uniform flow conditions.

tween uniform and non-uniform flow conditions, temporal variations of horizontal velocity component are compared in Fig. 11. V40 and K40 are time series of horizontal velocity measured in uniform and non-uniform flow conditions, respectively. It is obvious that the fluctuations have been damped in uniform conditions. In Figs. 12 and 13 the results have been categorized into uniform and non-uniform conditions to make them clearer. In both conditions fractal dimension and *Fr* has direct relation. Although the relationship between *Df* and *Re* is not clearly obvious, it seems that fractal dimension does not change significantly among different Reynolds number. In Fig. 14 fractal dimension of u', v', and $u'v'$ versus $Fr(d/H)$ for uniform and non-uniform flow conditions are plotted. In non-uniform conditions, fractal

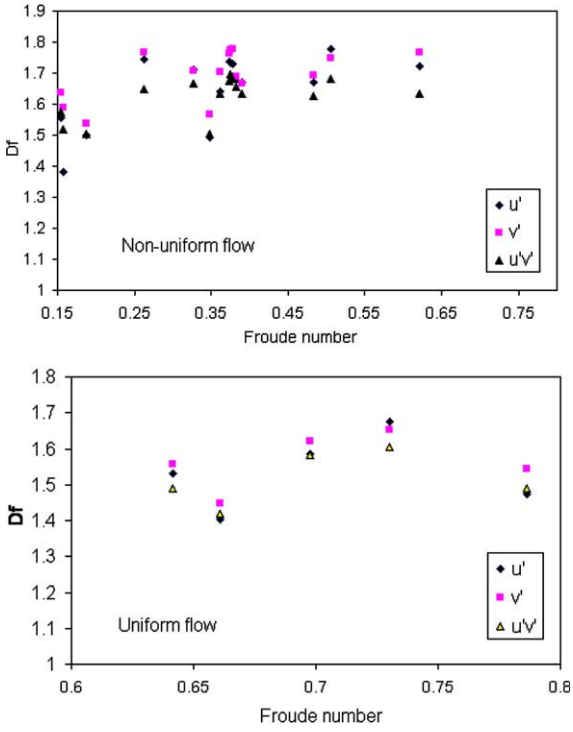

Fig. 13. Relationship between fractal dimension and Froude number in uniform and non-uniform flow conditions.

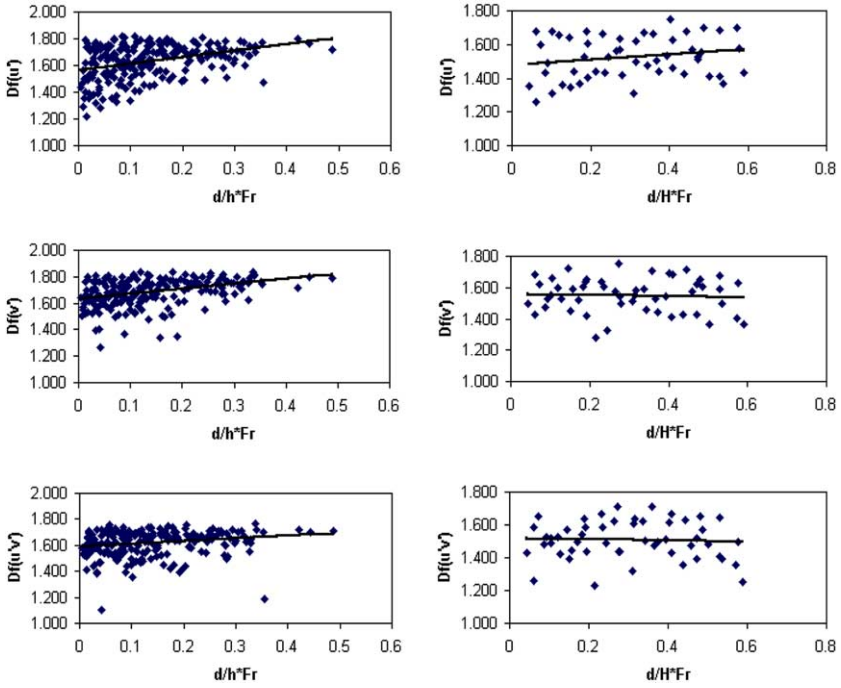

Fig. 14. Fractal dimension of u', v', and $u'v'$ versus $Fr(d/H)$ for non-uniform (left hand side graphs) and uniform (right hand side graphs) flow conditions.

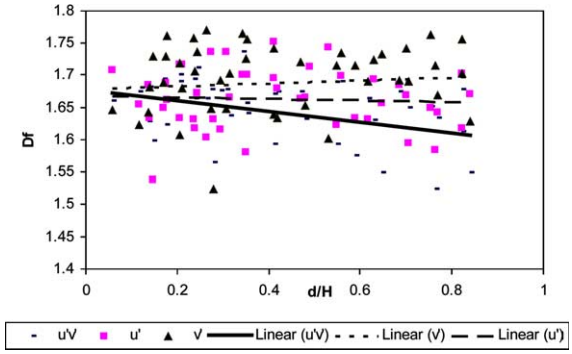

Fig. 15. Fractal dimension versus normalized depth.

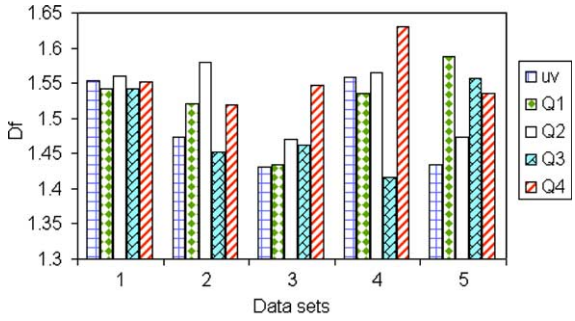

Fig. 16. Comparison of the fractal dimension of bursting events.

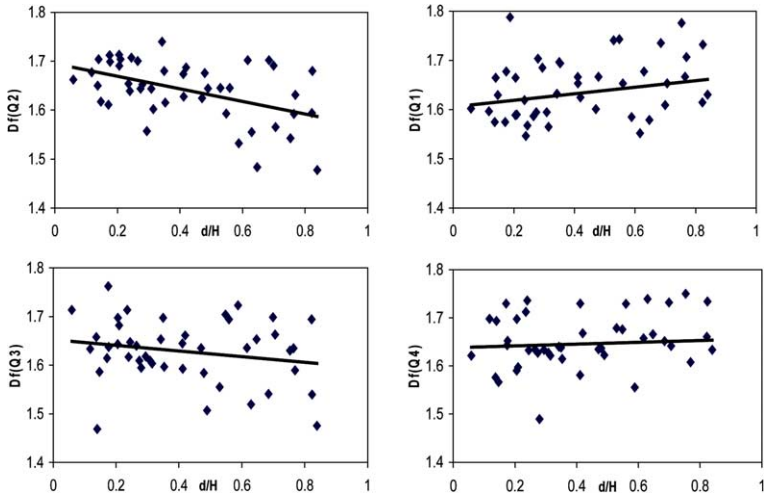

Fig. 17. Variations of fractal dimension over the flow depths in four quadrants.

dimension of both velocity fluctuation components and shear stress have a direct relation with $Fr(d/H)$, while in uniform flow these relations are somehow weaker. These results may be due to the effect of Fr. Since in uniform condition the range of Fr is more limited than non-uniform conditions. To omit the effect of Froude number, X, Y and YY tests, which have almost identical Fr, are selected and Df versus d/H are plotted in Fig. 15.

It has been found that the turbulence intensity in the longitudinal direction and Reynolds shear stress decreased from the bed to water surface while the turbulence intensity in the vertical direction did not change significantly over

the flow depth. As can be seen in Fig. 15, fractal dimension of u' and $u'v'$ decreased from the bed to water surface, while the fractal dimension of v' did not change significantly over the flow depth.

4.3. Fractal dimension of bursting events

In this study, fractal dimension of Reynolds shear stress in the four quadrants were computed for a number of data sets. These data sets were consisted of more than 2000 data points that was long enough to compute accurate fractal dimension in different quadrants. They are except from those tabulated in Table 1 and are shown with a number in Fig. 16. As it was expected, not only the fractal dimensions of quadrants were different but also the fractal dimension of the second and fourth (ejection and sweep) quadrants were greater than $Df(u'v')$ of combination of the all events. Although the results confirmed Keshavarzi's findings, but the number of data sets is limited and further investigation is necessary to improve this idea.

For X, Y, and YY tests, fractal dimension of Reynolds shear stress, $Df(u'v')$, over the flow depths in four quadrants are presented in Fig. 17. $Df(u'v')$ in sweep and inward interaction increased from the bed to the water surface while in the other two events $Df(u'v')$ changed reversely. In comparison of Figs. 17 and 15 it can be concluded that variation of $Df(u'v')$ in quadrants and its variation as a whole are not identical. Therefore, this difference should be taken into consideration for turbulence modeling using fractal dimension.

5. Conclusions

Fractal interpolation functions were successfully used to turbulence properties modeling. Extremum method found to be a good approach to find the desirable number of affine transformations. It was also more efficient than exhaustive search to find the optimum number of transformations. Moreover it was able to calculate accurate fractal dimension of the 1-d fractal curve with using the minimum number of data points (only 500 data points).

Time series of velocity fluctuation components and turbulent shear stress were approximated reasonably using fractal interpolation functions. The approximation can be improved by improving the extremum selection filters or even by selecting them manually. There were not a specific relationship between normalized depth and fractal dimension of turbulent data. Fractal dimension of u', v' and $u'v'$ were correlated to Froude number and somehow with Reynolds' number of the flow and these relationship were different in uniform and non-uniform flows. The fractal dimension of u', v', and $u'v'$ ranged from 1.4 to 1.8 and the average of them were 1.615, 1.657, and 1.559, respectively. These values can be used for turbulence modeling in open channel flows.

Fractal dimension of $u'v'$ among bursting events were different and they changed differently over the flow depth. Fractal dimension of $u'v'$ in sweep and ejection events were more than mean fractal dimension of $u'v'$. Finally it can be concluded that turbulence properties in open channel flow can be approximated by fractal theory.

References

[1] Richardson LF. Weather prediction by numerical process. London: Cambridge University Press; 1922.
[2] Einstein HA, Li H. The viscous sublayer along a smooth boundary. Transactions, ASCE, vol. 123, Paper No. 2992: 1958. p. 293–313.
[3] Praskovsky WF, Dabberdt EA, Praskovskaya EA, Hoydysh WG, Holynskyj O. Fractal geometry of isoconcentration surfaces in a smoke plume. J Atmos Sci 1996;53:5–21.
[4] Sreenivasan KR, Meneveau C. The fractal facets of turbulence. J Fluid Mech 1986;173:357–86.
[5] Meneveau C, Sreenivasan KR. The multifractal nature of turbulent energy dissipation. J Fluid Mech 1991;224:429.
[6] Scotti A, Meneveau C. Fractal dimension of velocity signal in high-Reynolds-number hydrodynamic turbulence. Phys Rev E 1995;51:5594–608.
[7] Scotti A, Meneveau C. A fractal model for larg eddy simulation. Physica D 1999;127:198–232.
[8] Frisch U, Sulem PL, Nelkin M. A simple dynamic model of intermittently fully developed turbulence. J Fluid Mech 1978;87(4):719–36.
[9] Jaw SY, Chen CJ. Near wall turbulence modeling using fractal dimensions. J Eng Mech ASCE 1999;125:804–11.
[10] Kline SJ, Reynolds WC, Schraub FA, Runstadler PW. The structure of turbulent boundary layers. J Fluid Mech 1967;30(4):741–73.
[11] Bridge JS, Bennett SJ. A model for entrainment and transport of sediment grains of mixed sizes, shapes and densities. Water Resour Res 1992;28(2):337–63.

[12] Thorne PD, Williams JJ, Heathershaw AD. In situ acoustic measurements of marine gravel threshold and transport. Sedimentology 1989;36:61–74.
[13] Nelson JM, Shreve RL, Mclean SR, Drake TG. Role of near-bed turbulence structure in bed load transport and bed form mechanics. Water Resour Res 1995;31(8):2071–86.
[14] Drake TG, Shreve RL, Dietrich WE, Whiting PJ, Leopold LB. Bed load transport of fine gravel observed by motion-picture photography. J Fluid Mech 1988;192:193–217.
[15] Keshavarzi AR, Ball JE. An application of image processing in the study of sediment motion. J Hydra Res 1999;37(4).
[16] Nezu I, Nakagawa H. Turbulence in open channel flows. Balkema, Rotterdam: IAHR Monograph; 1993.
[17] Nakagwa H, Nezu I. Bursting phenomenon near the wall in open channel flow and its simple mathematical model. Mem Fac Eng Kyoto University, Japan, XL (4) 1978;40:213–40.
[18] Grass AJ. Structural features of turbulent flow over smooth and rough boundaries. J Fluid Mech 1971;50(2):233–55.
[19] Keshavarzi AR. Entrainment of sediment particles from a flat mobile bed with the influence of near-wall turbulence. Ph.D. Thesis. University of New South Wales, Australia, 1997.
[20] Keshavarzi AR, Ball JE. An analysis of the characteristics of rough bed turbulent shear stress in an open channel flow. J Stochastic Hydrol Hydr 1997;11(3).
[21] Barnsley MF. Fractals everywhere. 2nd ed. San Deigo: Morgan Kaufmann; 1993.
[22] Strahle WC. Turbulent combustion analysis using fractals. AIAA J 1990;3:409–17.
[23] Marvasti MA, Strahle WC. Fractal geometry analysis of turbulent data. Signal Process 1995;41:191–201.
[24] Mazel DS, Hayes MH. Using iterated function systems to model discrete sequences. IEEE Trans 1992;40:1724–34.
[25] Vines G. Signal modeling with iterated function systems. Ph.D. Thesis. Georgia Institute of Technology, USA, 1993.
[26] Frederiksen RD, Dahm WJA, Dowling DR. Experimental assessment of fractal scale similarity in turbulent flows. Part 1. J Fluid Mech 1996;327:35–72.